mSense: Towards Mobile Material Sensing with a Single Millimeter-Wave Radio

CHENSHU WU, University of Maryland, College Park and Origin Wireless Inc.
FENG ZHANG, Origin Wireless Inc.
BEIBEI WANG, Origin Wireless Inc.
K. J. RAY LIU, University of Maryland, College Park and Origin Wireless Inc.

Target material sensing in ubiquitous contexts plays an important role in various applications. Recently, a few wireless sensing systems have been proposed for material identification. Yet, prior work usually requires to capture the signals penetrating a target (with devices set up on both sides of the target) or to instrument the target (*e.g.*, by attaching an RFID tag), relies on multiple transceivers, and/or involves unexplainable feature engineering. In this paper, we explore the feasibility of material identification by analyzing only the signals reflected off the target, rather than those penetrating it, with a single RF radio. We present `mSense`, a mobile material sensing system using a single millimeter-wave (mmWave) radio. At the core of `mSense` is the insight that different materials reflect RF signals in distinct ways. We propose a novel and easy-to-measure material reflection feature that quantitatively characterizes the material's reflectivity. A set of techniques are then devised to achieve accurate and robust material identification despite various factors, including device mobility, hardware defects of commodity mmWave radios, environmental interferences, and etc. Experiments using commercial mmWave networking chipsets demonstrate an average accuracy of 93% in categorizing five common types of materials: aluminum, ceramic, plastic, wood, and water, regardless of their different sizes and thicknesses. The accuracy retains about 90% even in mobile scenarios (*i.e.*, a user holds and moves the radio to perform sensing), which shows the great potential of `mSense` for mobile applications. A case study on 21 daily objects of various materials, shapes, and textures over different days further validates the performance in differentiating real-life objects.

CCS Concepts: • **Human-centered computing → Ubiquitous and mobile computing**.

Additional Key Words and Phrases: Material Sensing; Material Identification; Object Recognition; Millimeter Wave; Wireless Sensing; Contactless Sensing; Mobile Sensing

ACM Reference Format:
Chenshu Wu, Feng Zhang, Beibei Wang, and K. J. Ray Liu. 2020. mSense: Towards Mobile Material Sensing with a Single Millimeter-Wave Radio. *Proc. ACM Interact. Mob. Wearable Ubiquitous Technol.* 4, 3, Article 106 (September 2020), 20 pages. https://doi.org/10.1145/3411822

1 INTRODUCTION

Notable efforts have been made to enable material identification on ubiquitous computing machines. In recent years, the proliferation of autonomous vehicles and drones, in-home robots, and various smart devices has further driven such demand of material awareness in mobile environments. For example, material sensing could facilitate

Authors' addresses: Chenshu Wu, University of Maryland, College Park and Origin Wireless Inc., cswu@umd.edu; Feng Zhang, Origin Wireless Inc., feng.zhang@originwirelessai.com; Beibei Wang, Origin Wireless Inc., beibei.wang@originwirelessai.com; K. J. Ray Liu, University of Maryland, College Park and Origin Wireless Inc., kjrliu@umd.edu.

2474-9567/2020/9-ART106 $15.00
https://doi.org/10.1145/3411822

household waste sorting, enhance robots with ambient awareness, enrich environment mapping with object types and underpin novel interactive interfaces, etc. All these applications necessitate accurate material identification in ubiquitous and portable settings.

Unfortunately, conventional systems usually rely on specialized hardware like X-Ray and ultrasonography and are limited to only critical security and medical usage, preventing them from ubiquitous adoption outside a lab environment. Recently, as wireless sensing emerges, low-cost radios have been exploited to classify materials [14, 30, 39], such as RFID [30] and UWB radar [12] for liquid testing. These works, however, usually rely on multiple transceivers locating on different sides of the target to measure the signals penetrating it, limiting their applications to only fixed, constrained setups and to objects that RF signals can penetrate through. Some other works use one single device [10, 37] by feeding the raw signals into machine learning models, but do not extract explainable material features. The latest work [39] utilizes WiFi reflection signals, yet needs multiple customized devices. Other works on wireless sensing have employed RF signals to detect and track targets [8, 25, 27], but do not address their material types. In this work, we ask this research question: *Is it feasible to estimate the material's reflection property and accordingly identify the material from only the reflection signals measured by a single off-the-shelf radio?*

Recently, mmWave radios have emerged as the next-generation wireless communication technique and are becoming more widely available on commodity networking devices [3, 5, 6]. Meanwhile, research efforts have also been devoted to a rising trend of joint radar communication systems [17, 22, 42]. This paper presents the design and implementation of `mSense`, a *mobile material sensing* system for ubiquitous environments that leverages these two opportunities by reusing a 60GHz networking radio as a mmWave radar. Unlike existing systems that mostly rely on penetrating signals and/or multiple transceivers, `mSense` exploits only the signals reflecting off the target and employs a single 60GHz mmWave radio. The key insight is that different objects, depending on their specific materials, reflect the incident electromagnetic waves at distinct extents, *e.g.*, metals typically reflect much more energy than woods. To identify the target material, a user simply needs to point the radio relatively perpendicular towards the target. `mSense` then measures the Channel Impulse Response (CIR), from which it will automatically determine the material type. Different from existing works [10, 12], `mSense` circumvents the need to put up two or more radios on lateral sides of the target or to instrument it with extra device, thus allowing ubiquitous usage and promising a mobile and flexible solution that might ultimately enable a smartphone, should it be equipped with a mmWave radio in the future, to perform target material sensing everywhere.

`mSense` models the signal propagation by accounting for the reflection coefficient, an intrinsic property of the material. It then derives a novel *material reflection feature* (MRF) that quantitatively characterizes the material's reflectivity and accordingly associates the target's material type. The proposed MRF turns out to be independent of the environments, the propagation distance, and target sizes and thicknesses, etc., and thus allows material sensing in mobile contexts with flexible setup. However, it is challenging to estimate the MRF precisely and reliably. Particularly, the CIR measured on our mmWave platform offers inadequate range resolution (4.26 cm given the bandwidth of 3.52 GHz), contains timing drifts, and suffers from considerable measurement noises, all leading to errors in estimating the propagation distance and the signal amplitude. To overcome these challenges, `mSense` first interpolate the measured CIR to improve the range estimation to the sub-centimeter level. We then propose a novel synchronization scheme by leveraging the direct path, *i.e.*, direct leakage between the co-located transmitter (Tx) and receiver (Rx), to synchronize all the CIRs. By employing noise cancellation, we eliminate the hardware distortions and measurement noises and obtain the components that only relate to the target reflection. Then we perform target detection on the sanitized CIR to estimate the accurate propagation distance and the corresponding amplitude response and accordingly calculate the MRF. We further exploit the spatial diversity attributed by the large antenna arrays to facilitate the robustness. And finally, `mSense` determines the material type by looking up the best-matched record in a prior database with the estimated MRF values.

We implement a prototype of mSense on a Qualcomm testbed, which enables radar-like operations on a commodity 60GHz 802.11ad/ay networking chipset by attaching one additional antenna array, each consisting of 32 antennas. We first conduct experiments using this testbed to validate the performance on five common types of materials: metal (aluminum), plastic, ceramic, water, wood. The results show that mSense achieves an average identification accuracy of 92.87%, regardless of the various target sizes, thicknesses, and distances to the device. More importantly, the accuracy retains 89.36% in mobile scenarios where a user holds and moves the device for sensing. We also perform a case study of a set of 21 daily objects of different materials, such as tables and desks, plastic mats, painted objects, etc., over different days. The results show mSense achieves reasonable performance for everyday object recognition despite the various compositions, shapes, surface textures, and hardness, etc. Using only the reflection signals measured by a mobile radio, we believe mSense takes an important step towards mobile material sensing for everyday usage. Also, our practice on the radar platform that reuses a networking device sheds light on the emerging joint radar communication systems, which may promise a future paradigm of wireless communication and sensing.

In summary, the core contributions of this paper are as follows:

- We present the first-of-its-kind system mSense that demonstrates the feasibility of mobile material sensing based on the reflection signals measured by a single mmWave radio. We introduce a novel MRF that characterizes the target's intrinsic reflectivity and thus associates the material type.
- mSense devises a pipeline of techniques to estimate the MRF robustly and accurately, including CIR interpolation, direct path based synchronization, background and noise cancellation, etc., which may also benefit various mmWave sensing applications beyond material identification.
- We prototype mSense by reusing a commodity 60GHz networking chipset as a radar and validate the performance in both static and mobile cases with common materials and daily objects.

Next, we present the design space and potential applications in §2. We present the preliminaries in §3 and detail the design in §4. The implementation is described in §5, followed by experiments in §6 and discussions in §7. We review the literature in §8 and conclude in §9.

2 DESIGN SPACE

2.1 Potential Applications and Design Goals

Mobile material sensing in ubiquitous contexts would enable different applications. It could facilitate household waste sorting, a common sustainability practice in many countries, which would otherwise be inefficient since daily objects made up of different materials may look similar or indifferent to users. It would improve home security by detecting water leakage, or enable a microwave oven to detect metals inside and warn the user. Metal detection is also useful for suspicious object checking [28] and autonomous drones [39]. Applications also extend to robots, drones, and machines, which can adaptively adjust their actions according to the material types of surrounding objects. For example, robots could apply different grip strengths for ceramic or metal targets, and an electric saw could automatically and immediately stop itself if it could detect skin. Indoor mapping robots could map not only the environment layouts but also the obstacle types. With material awareness, educational toys could instruct kids to perceive the physical world in more interactive ways, e.g., changing the functions based on the materials being touched [37]. Further, as mmWave radios become available on smartphones [4], we could imagine smartphones as ubiquitous equipment for daily material sensing, which could better benefit more people, such as the visually impaired who might have difficulties distinguishing certain materials by touch.

mSense aims to offer ubiquitous material sensing in mobile environments, without dedicated hardware or the cumbersome setup, for these applications. Utilizing only the reflection signals on commodity mmWave chipsets, however, we do not target at highly precise, critical material identification but mainly focus on daily objects with ordinary materials like metals, plastics, woods, etc. In general, the types of materials that can be differentiated by

RF could be limited (Notable confusion exists even using penetration signals due to the close RF responses [12]). But recognizing a limited number of materials could be already useful [28, 39]. Albeit differentiating certain types of materials may look simple to humans, it lacks such a technique for ubiquitous devices even to tell metals from woods easily. We believe enabling such a capability for ubiquitous devices would trigger new applications, and clearly, the design of mSense takes an essential step towards the goal.

2.2 Why 60GHz Networking Radio?

The past years have seen an explosion in wireless sensing [8, 10, 14, 25, 27, 44], which basically brings some radar-like features indoors by reusing radio signals purposed for communication. Dedicated radars are also becoming popular for indoor and mobile applications. Apple and Google have equipped their latest phone models with UWB radar [7] and mmWave radar [4], respectively. Another research trend is the synergistic design of communication and radar systems that use the same hardware and spectral resources for the dual functions [17, 22]. 60GHz mmWave radios, with the large bandwidth and phased antenna array, is promising for such systems [22]. 60GHz WiFi, standardized as 802.11ad/ay [5], is available in commodity routers [6] and is being integrated into smartphones and vehicles [1, 2]. The industry is also actively exploring radar capabilities by reusing the 60GHz radios [1]. For example, the device we use in this work is from Qualcomm, which provides a radar-like mode on top of a commodity 60GHz networking chip. Such a dual networking and radar device has distinct advantages since it reuses the networking device and will immediately serve a ubiquitous radar when 60GHz WiFi is widely deployed. It promises higher quality signals for wireless sensing compared to the 2.4GHz/5GHz WiFi [34, 39].

The second reason for using 60GHz radio is our design choice of using reflection signals only. A bottleneck preventing existing solutions from ubiquitous applications is that they require a special setup with two or more transceivers on both sides of the target [12–14, 30, 39] or with tags attached to the target [16, 35]. In addition to the inconvenience, the use of penetrating signals imposes two fundamental issues: 1) EM waves decays differently with respect to the propagation distance d in different media (*e.g.*, lossy media vs. lossless media). For example, the amplitude decreases linearly with respect to $1/d$ in free space and approximately in air, while, differently, experiences exponential decrease over d in a lossy media. To deal with the problem, prior works either apply a universal model for different medias present in the propagation path [14, 30] or assume a specific category of materials (particularly different liquids [12, 14]). 2) For conductive materials (*e.g.*, metals, graphite), RF signals may not penetrate the target. Neither can wireless signals, especially those at mmWave frequency bands, penetrate very thick objects. In mSense, we resort to mmWave signals and exploit only the reflection signals for analysis to circumvent the two issues and improve the system usability. The problem becomes more challenging than using the penetrating signals since the reflection signals have not passed through the material.

3 MATERIAL REFLECTION FEATURE

This section presents the basic principles and introduces a novel MRF to measure the object reflectivity.

3.1 The Basic Principle

For an EM wave propagating in free space, the signal amplitude decreases as the inverse of the propagation distance d, which is well modeled by the Friis Transmission Formula[1] as:

$$A_d = A_0 g_t g_r \frac{\lambda}{4\pi d}, \tag{1}$$

[1]We use the signal amplitude for consistency here, yet the Friis Transmission Formula is more often defined in its power form, *i.e.*, $P_r = P_t G_t G_r \lambda^2/(4\pi d)^2$, where P_t and P_r denote the transmit and receive power, and G_t and G_r indicate the power gains of the transmit and receive antennas, respectively.

where A_0 denotes the amplitude of the transmitting signal, A_d denotes the received amplitude at propagation distance d, g_t and g_r are the transmitting and receiving antenna gains, respectively, and λ is the wavelength. The above model generally applies to air propagation, which is approximated to free space propagation. In practice, due to multipath effects, an additional exponential component may be applied to d, which is not the case for 60GHz signals with few multipath.

When the EM wave encounters a material boundary, causing an impedance discontinuity in the propagation medium, the incident energy will be partially reflected back and partially transmitted into the new material. The ratio of the amplitude of the reflected wave to that of the incident wave is given by the *reflection coefficient*, denoted as r:

$$A_{\text{out}} = A_{\text{in}} \cdot r, \tag{2}$$

where A_{in} and A_{out} denotes the amplitudes of the incoming and reflecting signals respectively. At normal incidence, the reflection coefficient r is, according to the Fresnel Equations, expressed as $r = \frac{n_2 - n_1}{n_2 + n_1}$, where n_1 and n_2 are the *refractive indices* of the incident and transmitted materials, respectively. The refractive index n of a material is defined as the ratio of the speed of light in vacuum, c, and the speed of EM waves in the propagation medium, v: $n = \frac{c}{v}$. The refractive index n is an intrinsic characteristic of a material related to the material's complex permittivity $\epsilon_r = \epsilon_r' + \epsilon_r''$ [26]: $n = \sqrt{\frac{1}{2}(\sqrt{(\epsilon_r')^2 + (\epsilon_r'')^2} + \epsilon_r')}$. Typically the incident material is air, for which we have $n_{air} = 1$. And thus r becomes $r = (n-1)/(n+1)$, where n denotes the refractive index of the target material.

For the EM wave that continues to travel inside the target, assuming a uniform lossy media, its amplitude experiences exponential decrease over the propagation distance d:

$$A_{d_{\text{in}}} = A_{\text{in}} e^{-\alpha d_{\text{in}}}, \tag{3}$$

where $A_{d_{\text{in}}}$ denotes the amplitude at distance d_{in} to the target surface and and A_{in} denotes that at the incident surface. α is the *attenuation constant* that depends on the intrinsic material properties. As can be told from (3), α is defined as the inverse of a distance δ, often called the skin depth (or penetration depth), over which the strength of the electromagnetic field decays to $1/e = 0.368$ of its original value.

Similar to the refractive index, the attenuation constant α is also related to the material's intrinsic relative permittivity: $\alpha = \frac{2\pi}{\lambda_0}\sqrt{\frac{1}{2}(\sqrt{(\epsilon_r')^2 + (\epsilon_r'')^2} - \epsilon_r')}$. Thus, if n and α are available, the above two equations can be jointly solved to derive the two unknowns, i.e., ϵ_r' and ϵ_r''. In fact, some of the existing works attempt to resolve these parameters for material sensing by analyzing the signals penetrating a target, yet require a special setup in order to capture the penetrating signals [12–14, 30]. As a consequence, while prior works have brought material sensing out of the traditional lab environments, they are still not sufficient for ubiquitous mobile environments.

3.2 Material Reflection Feature

Since we resort to only the reflection signals, the attenuation constant and permittivity can no longer be extracted. Instead, we propose a novel metric related to the material's reflectivity property, termed as the *material reflection feature*, which could be effectively extracted from the reflection signals. Recall Eqn. (1) and (2), the received amplitude at the Rx, which is co-located with the Tx, can be expressed as

$$A_d = A_0 g_t g_r \frac{\lambda}{4\pi(2d)} \cdot r \propto \frac{r}{d}. \tag{4}$$

The above expression accounts for the round-trip propagation distance $2d$ and the reflection coefficient r of the target. Note that here d denotes the range of the target (see Fig. 2), *i.e.*, the distance from the target surface to the radio. Let $A_d \triangleq \gamma \frac{1}{d}$, then we have

$$\gamma = A_0 g_t g_r \frac{\lambda}{8\pi} \cdot r = A_d \cdot d. \tag{5}$$

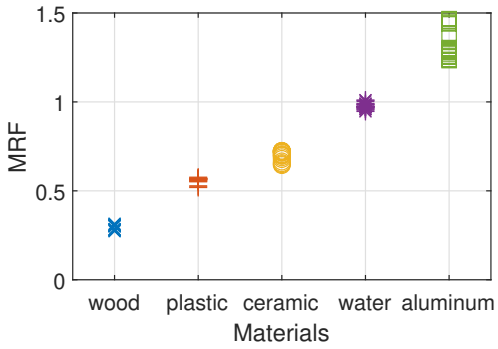

Fig. 1. The MRF of five common materials

The defined γ has the following properties:

- First, γ is a linear function of the target reflection coefficient r, an intrinsic characteristic of the target material, and is independent of the propagation distance. As shown by the middle term, except for three constants, *i.e.*, the transmitting amplitude A_0, the Tx and Rx antenna gains g_t and g_r[2], γ is only related to the reflection coefficient r and is thus unique to a particular material.
- Second, implied by the right term, we can easily estimate γ as long as we obtain the range d of the target and the corresponding signal amplitude A_d.

As a result, we term γ as the MRF and employ it for material identification, successfully avoiding the need of knowing the precise A_0 to derive r. In practice, only an estimated version of γ, denoted as $\hat{\gamma} = \hat{A}_d\hat{d}$, can be obtained, where $\hat{d}$ and $\hat{A}_d$ are the estimated target range and the corresponding measured amplitude, respectively. As shown in Fig. 1, we demonstrate by preliminary measurements that γ is discernible, reliable, and accurate in distinguishing different material types. The stronger the target reflects the incident signals, the larger MRF values it has. And albeit small variances exist, the measured MRFs of the exemplified materials are obviously set apart.

In below, we present the pipeline to process the CIR measurements on the 60GHz WiFi radio that overcomes multiple challenges and eventually outputs precise estimation of γ. Evidently, the key is to estimate the range d and the amplitude response A_d accurately.

4 MSENSE DESIGN

4.1 Overview

mSense consists of two stages: a training stage that constructs a database of different materials and a testing stage that tests a target by matching against the database. As shown in Fig. 2, mSense collects CIRs when the user points the radio towards a target (roughly perpendicularly). The raw CIRs are first interpolated to improve range accuracy and then synchronized. Noise cancellation is employed to eliminate the hardware distortions and measurement noises. We then perform target detection to obtain the amplitudes and distances from all available antenna pairs, from which we estimate a novel MRF. Finally, we determine the material type by finding the best match against the pre-trained database storing the MRF of different materials.

4.2 60GHz WiFi Radio As a Radar

We first introduce our experimental testbed and characterize the CIR measurements from it.

[2]Later in our implementation, we will take out the antenna gains g_t and g_r as well, which are available on our testbed. Thus there will be only one constant A_0 remained.

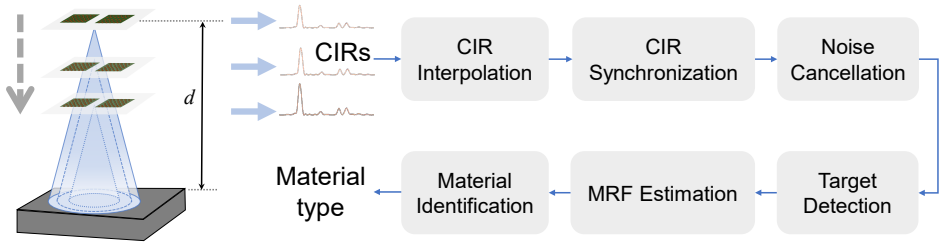

Fig. 2. Overview of the mSense workflow

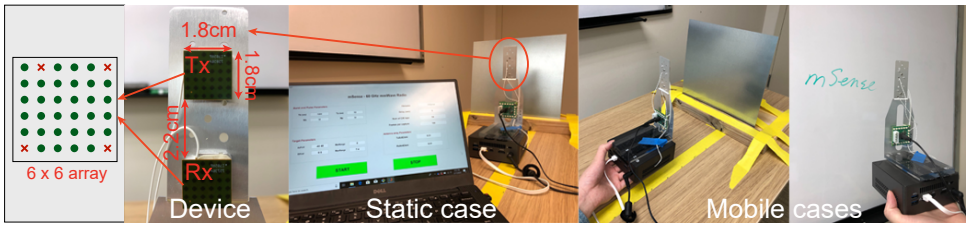

Fig. 3. mSense testbed and example usage scenarios

Radar Function on 60GHz WiFi Radio The design reuses commodity Qualcomm 802.11ad chipsets by attaching an additional array to enable full-duplex radar-like operation. The Tx array and the Rx array are co-located, each equipped with 32 elements arranged in a 6×6 layout, as shown in Fig. 3. In the radar mode, the Tx transmits pulse signals and the Rx receives the reflection signals and estimates the CIR, which is much more accurate than that reported by previous work [23] under networking mode. However, different from a true radar, the Tx and Rx arrays do not transmit and receive concurrently. Instead, a Tx element transmits pulses to each of the 32 Rx elements in turn, each pulse taking as short as 1 us, and next Tx element continues.

In the normal networking mode, the extra array provides additional spatial diversity or is simply unused. Typically, the radar sensing only requires minimal time. Thus the radar and networking modes can rapidly switch in time to achieve dual functions "simultaneously". To our best knowledge, the testbed is the first real-world implementation of a radar system built on top of a commercial networking chipset. In this paper, we only focus on the platform's radar capability and operate it like a radar.

CIR on 60GHz Radio A CIR profiles the propagation delays and the channel responses of different signal paths between Tx and Rx, which is denoted by

$$h(\tau) = \sum_{l=1}^{L} a_l e^{-j\theta_l} \delta(\tau - \tau_l), \tag{6}$$

where a_l, θ_l, and τ_l are the amplitude, phase and time delay of the lth path, respectively. L is the total number of paths and $\delta(\tau)$ is the Dirac delta function. Fig. 4 shows an example of the CIR measured by our mmWave device. Each impulse tap of a CIR, $h(\tau_l)$, represents a delayed multipath component. Note that our device uses a bandwidth of 3.52 GHz centered at 60GHz frequency band, resulting in a ToF resolution of 0.28 nanosecond which, given the speed of light $c = 3 \times 10^8 m/s$, corresponds to a range resolution of 4.26 cm (for reflecting paths).

Compared to 2.4GHz/5GHz WiFi, the CIR of 60GHz mmWave signals offer distinct advantages due to the many antennas, large bandwidth, and high carrier frequency. However, applying the reported CIR for material sensing entails practical challenges. While the high range resolution is impressive for indoor localization [34], it is inadequate for material sensing. Furthermore, as demonstrated by our experimental measurements in the next

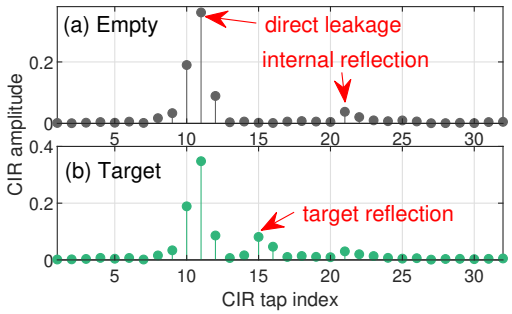

Fig. 4. CIR measurements without and with a target. The direct leakage appears at the 11th tap. When a target presents at about 17cm away, the amplitude around the 15th tap responsively increases.

section, the device contains considerable noises and exhibits unreliable amplitudes, making the material sensing even challenging. Specifically, as illustrated by Fig. 4 that shows the respective CIR measurements in the cases with and without a target in the field of interests, there are a few major problems with the CIR estimation with the present implementation of the radar-like radio:

- Limited range resolution: The physical range resolution of 4.26 cm is inadequate for precise MRF estimation.
- Synchronization errors: The reported CIR measurements over time might be out of synchronization.
- Measurement noise: Ideally, the CIR should be all nearly zeros in absence of reflection objects. As shown in Fig. 4, the CIR measurements contain strong *direct leakage*[3] from the Tx to the co-located Rx and notable *internal reflection*, significantly interfering the measurements in presence of a target.

In below, we present how `mSense` tackles these issues and enables mobile material sensing.

4.3 CIR Interpolation

To obtain finer details, we propose to up-sample the raw CIR via interpolation. The idea is similar to the interpolation in [12]. As illustrated in Fig. 5(a), however, if interpolating the CIR directly on the complex plane, the resulted amplitude and phase may not necessarily be smooth and uniform due to the coupled amplitude and phase. In addition, as shown in Fig. 5(c), interpolation on the phase does not produce meaningful results due to the ambiguity: Given two adjacent taps, the distance separation is 4.26 cm, within which the phase could have rotated for over 8 times. Since `mSense` mainly utilizes CIR amplitudes for material identification, we perform spline interpolation on the amplitude, which subsamples the amplitude effectively, as illustrated by Fig. 5(b).

Obviously, the interpolated CIR has denser sample points and peak tap of a particular path tends to be close to the real maximum tap value. Thereby, the interpolation offers finer granularity in delay (and thus range) and amplitude estimation, both of which are critical to material identification. In `mSense`, we perform 8x interpolation, promoting the ToF precision to 35.2 picoseconds and the distance precision to 0.52 cm. Fig. 6 illustrates an example with 2× and 16× interpolation of the original CIR.

4.4 CIR Synchronization

The default synchronization of the 60GHz radio is not precise enough due to the resolution limit (*e.g.*, misalignment of one tap would lead to an offset of 4.26 cm in distance estimation). Neither is the synchronization reliable, *i.e.*, the leakage tap would vary over time (especially due to temperature changes) and even over antenna pairs.

[3]The Qualcomm implementation roughly sets the direct leakage to the 11th tap, which could be at any tap principally.

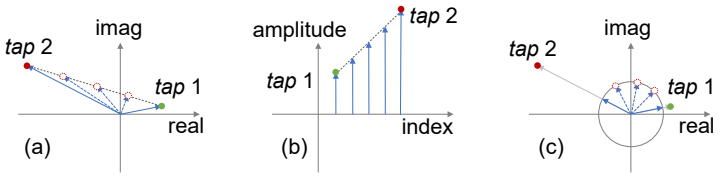

Fig. 5. Interpolation of complex CIR. Interpolation on (a) complex plane with coupled amplitude and phase, (b) the amplitude, and (c) the phase. Linear interpolation is used for simple illustration.

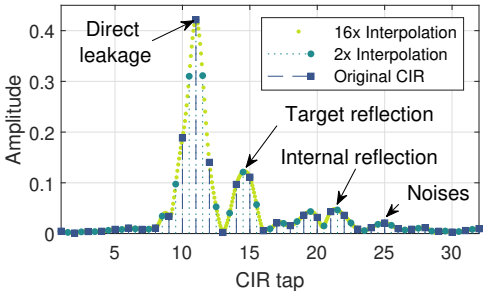

Fig. 6. An example of CIR interpolation

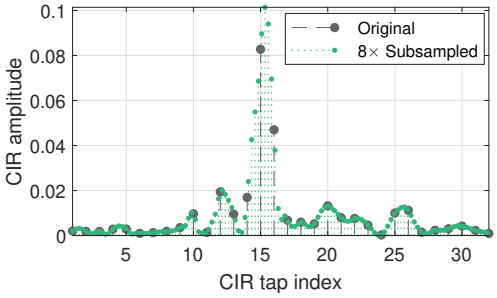

Fig. 7. An example of noise cancellation

To synchronize all the CIRs more precisely and reliably, we leverage the direct leakage from the Tx to the Rx. The key insight is that the direct leakage between the co-located Tx and Rx is free of multipaths and produces a fixed time of flight (about 0.13 nanoseconds in our platform with a separation of about 4 cm between the Tx and the Rx). Thus the direct leakage tap can serve as a reference tap, and we align this leakage tap of all CIR measurements to synchronize them and derive the relative ToF of each subsequent tap. Later we will obtain the absolute ToF for range estimation by compensating the ToF of the direct path from a specific Tx-Rx link on top of the relative ToF, as detailed in Section 4.6.

We first select one reference CIR whose direct leakage tap is assigned to a specific tap, denoted as the l_0th tap. Then for each CIR, we correlate it with the reference CIR. The correlation only involves the first L_0 taps that cover the direct leakage but exclude the other taps that potentially associate with target or background reflections. Since the direct leakage keeps relatively stable with a similar pattern for different measurements, the tap at which the maximum correlation occurs is declared as the direct leakage tap. And the CIR is accordingly synchronized by shifting the direct leakage tap to the l_0th tap, if they are different. To maintain the same length of the CIR, we perform circular shift for the alignment, which could alternatively be achieved by padding zeros to the first (or last) taps. The interpolated CIR is used here for the sake of finer-grained delays.

We note that the proposed synchronization technique is also applicable to the general case of 60GHz networking with unsynchronized, separate Tx and Rx devices. As long as the LOS distance between the Tx and Rx is known and fixed, the measurements can be synchronized by referring to the LOS delay.

4.5 Noise Cancellation

Fig. 4 also shows the CIR measured on the commercial 60GHz networking device contains considerable interferences and noises. In addition to the direct leakage that we utilized for synchronization, there is *internal reflection* due to the intermediate frequency (IF) cable connectors, which occurs around 2.8 ns (corresponding to a range around 42.6 cm) as shown in Fig. 4. To combat the impacts of these interferences and noises, we propose to cancel them out to obtain the CIR components only related to the target reflection.

The CIR can be modeled as the sum of the components reflected off the target, denoted as h^{t} and the components contributed by the direct leakage, internal reflection, measurement noises, and background reflection if any, denoted as h^{n}. To obtain h^{t} from the measured h, we utilize a reference CIR measured with no target in the field of interest, which characterizes the components h^{n}. Such a reference CIR can be easily obtained by collecting measurements when the device is pointing towards the air without the presence of the target. Say there are Q such measurements, h^{n} will be estimated as the average sample, *i.e.*, $h^{\mathrm{n}}(\tau_l) = \frac{1}{Q}\sum_{i=1}^{Q} h(\tau_l, t_i)$.

Then we subtract h^{n} from a new h measured at time t towards a target and obtain h^{t}. Since the measured CIR amplitudes may slightly vary over time due to the automatic gain control (AGC), we apply a scaling factor β for complete cancellation:

$$h^{\mathrm{t}}(\tau, t) = h(\tau, t) - \beta h^{\mathrm{n}}(\tau). \tag{7}$$

Assuming that the direct leakage should be constant, the scaling factor is computed based on the first L_0 taps concerning only the direct leakage and noises by minimizing the mean square error (MMSE):

$$\beta^{\star} = \arg\min_{\beta} \sum_{l=1}^{L_0} |h(\tau_l, t) - \beta h^{\mathrm{n}}(\tau_l)|^2. \tag{8}$$

Fig. 7 shows an example of the CIR after the noise cancellation. Compared to Fig. 4(b), the amplitude of the target reflection spikes while those of the direct leakage and internal reflection are greatly eliminated, with residuals only slightly higher than the noises.

The cancellation is mainly used to remove the hardware distortions and measurement noises, rather than the background-tailored interferences. Therefore, the reference CIR can be a one-time calibration and does not need to be measured for every data capturing session, which largely consolidates its practical usage in mobile environments. In practice, it is possible to automatically collect the reference CIR since our system can detect whether there is a target within the range of interests (*e.g.*, within 1 meter); If none, the corresponding CIR samples can be used to generate the reference CIR. Note that although distant objects in the background (*e.g.*, walls, furniture, etc) may also reflect signals to be included in the reference CIR, they do not affect `mSense` since they are typically out of the range of interests.

4.6 Material Reflection Feature Estimation

We now detect the precise range and amplitude response of the target. Given that the direct leakage and internal reflection have been eliminated, we simply locate the CIR tap that holds the maximum amplitude as the one where the target presents at and accordingly derive the relative ToF Δt corresponding to that tap. The associated amplitude is taken as the amplitude of the signals reflected by the target.

The ToF Δt derived from the synchronized CIR is the relative value referenced to the direct leakage tap. Hence we need to compensate the direct leakage delay to obtain the absolute ToF. Given the geometry of the Tx and Rx antenna arrays, the separation distance between each pair of Tx and Rx antennas can be obtained in prior and the direct propagation delay can thereby be derived on top. For the M Tx antennas and N Rx antennas, define an $M \times N$ matrix S to represent the Tx-Rx separation distances, with $s_{m,n}$ denoting its entry at the mth Tx element and the nth Rx element, where $m = 1, \cdots M, n = 1, \cdots, N]$. Then given the measurements between the mth Tx antenna and the nth Rx antenna, the range of the target can be computed by

$$d_{m,n} = \frac{c\Delta t_{m,n} + s_{m,n}}{2}. \tag{9}$$

Here we take half of the propagation distance as the range since we assume normal incident, *i.e.*, the device is pointing to the target approximately at elevation 0°.

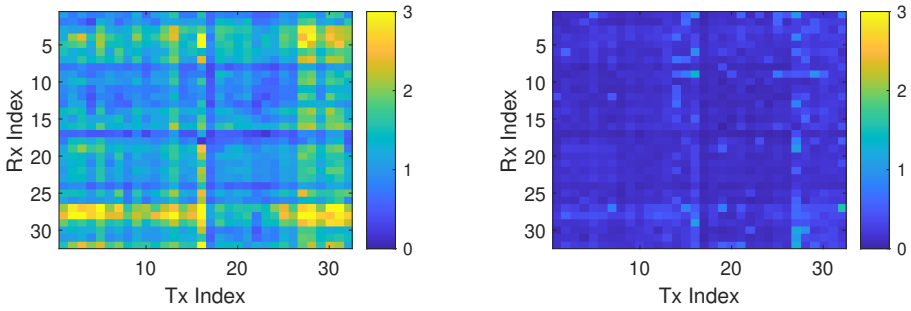

(a) MRF matrix of aluminum (b) MRF matrix of wood

Fig. 8. MRF matrix. The MRF matrix estimated by 32×32 antenna pairs. The same color range is used for the two matrices, showing that aluminum reflects much more energy than woods.

We perform the above target detection for the CIR measured by every pair of Tx-Rx antennas and obtain $M \times N$ estimates of γ in total, each denoted as $\gamma_{m,n} = \frac{A_{m,n} d_{m,n}}{g_t g_r}$ for the mth Tx element and the nth Rx element, where $A_{m.n}$ is the amplitude estimate at $d_{m,n}$ and g_t, g_r are the AGC gains reported by the device. Fig. 8 illustrates an example of the results. We then leverage the antenna diversity to achieve a more robust estimate of γ by removing potential outliers in the target detection. Specifically, we exclude those tuples whose distance estimate $d_{m,n}$ deviates from the majority of all the $M \times N$ estimates.

$$\hat{\gamma} = \frac{1}{|\mathcal{S}|} \sum_{(m,n) \in \mathcal{S}} \gamma_{m,n}. \tag{10}$$

Here $\mathcal{S}$ is defined as the set of tuples (m, n) that satisfy $||d_{m,n} - \tilde{d}|| \leq \delta, m = 1, \cdots, M, n = 1, \cdots, N$, where δ is a threshold set to the default range resolution, *i.e.*, $\delta = 4.26$ cm, $\tilde{d}$ is the median of all $d_{m,n}$.

`mSense` needs only one single frame to yield an estimate of the MRF γ. In case there are multiple frames over time, we will further improve the estimation by taking their average $\bar{\gamma} = \frac{1}{K} \sum_{k=1}^{K} \hat{\gamma}(k)$, where $\hat{\gamma}(k)$ is the estimation from the kth CIR frame and K is total number of available frames. Note that the device could be either moving or static during the measurements of successive frames.

4.7 Material Identification

Two steps are involved to identify material: An offline step to construct a database of the MRF for different materials; and an online step that retrieves the best matches for a given target. Given a set of materials of interests, we perform a "scan" on each of them and store the distribution of the estimated γ. To reduce the data amount needed for training, we build a histogram, rather than fitting a certain distribution, for each material type T, denoted as $\{<\gamma_i(T), p_i(T)>, i = 1, 2, \cdots, P\}$, where $\gamma_i(T)$ is the bin value and $p_i(T)$ is the corresponding probability (normalized count of observations), and P is the total number of bins. Note that a median filter is applied to remove the outlier estimates from the training samples in prior to building the histogram. Let $\mathcal{T}$ be the set of materials considered. Then in the online operating stage, for each material with γ to test, we find the best matching as follows:

$$T^{\star} = \arg\min_{T \in \mathcal{T}} \sum_{i=1}^{P} ||\gamma - \gamma_i(T)|| \cdot p_i(T). \tag{11}$$

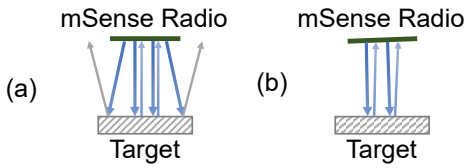

Fig. 9. Specular reflection. (a) Since mmWave signals mainly undergo specular reflection, the size of the target does not affect the performance as long as it is comparably larger than the antenna array. (b) Similarly, slight rotation in the array orientation will change the reflections, yet only produces negligible changes in propagation distances and thus does not affect the amplitude response a lot.

Besides, we apply an additional rule to check the "null" class, *i.e.*, unseen materials. Specifically, a material is claimed to be "unknown" if its MRF $\gamma < \min_{i=1,\cdots,P} \gamma_i(T)$ or $\gamma > \max_{i=1,\cdots,P} \gamma_i(T), \forall T \in \mathcal{T}$.

5 IMPLEMENTATION

Now we present the implementation details and discuss several issues concerning the practicability.

Hardware setup. We build an `mSense` prototype by using a 60GHz platform sponsored by Qualcomm. As shown in Fig. 3, the platform is equipped with a single commodity Qualcomm 60GHz 802.11ad chipsets. Different from common 60GHz networking radios, an extra antenna array is attached to the chip to enable the dual radar function. The Tx and Rx arrays are co-located with a 4 cm separation, each containing 32 antennas as a 6×6 phased array. To fit `mSense` for mobile devices, the testbed needs a much smaller form factor, which is more about the hardware design and will not influence the principles.

Recent efforts on 60GHz mmWave radios only report RSS together with the beam information. Very differently, our mmWave radio reuses a 60GHz networking chipset as a mobile radar and reports precise CIR. We believe such a dual function implementation sheds light on the integrated design for mmWave networking and sensing, and we hope the platform will become commercially available soon.

Software The radio is connected to a Linux host machine and the measured CIRs are sent out from there via an Ethernet cable to a Windows laptop. One can run Matlab to receive and process the CIR data in real time. Currently, we use Matlab to both collect CIR and implement `mSense` algorithm.

Specular Reflection A major problem for mmWave sensing is the specular reflection, which may lead to missing detection of the target. In `mSense`, however, specular reflection turns out to be an advantage that makes it more practical in mobile environments. First, as shown in Fig. 9(a), `mSense` becomes independent of the target size, as long as it is comparably larger than the radio size, which is 1.8 cm × 6 cm including the Tx and Rx arrays. Due to the specular reflection, reflections outside the area that the radio is perpendicularly facing are unlikely received, and thus do not affect the material sensing. Consequently, `mSense` can work with most daily objects whose size are generally larger than the radio.

Second, we request the user to point the radio perpendicularly to the target surface. In practice, it is impractical to ensure perfect normal incident, especially when a user is holding the radio in hand. Nevertheless, as shown in Fig. 9(b), although minor distortions in the radio orientation alter the signal propagation, the impacts on the received amplitude, which we leverage for material identification, are negligible. The reason is that such distortions only produce slight changes in the propagation distance, thereby keeping the received amplitude nearly unchanged. We further perform real-world measurements to verify the specular reflections. We set up a wide aluminum sheet and put the device at a distance of 20 cm to the target. We first rotate the device from the orientation of -60° to 60° and record the signals in Fig. 10a. As seen, the amplitudes drastically decrease when the device's orientation deviates far from the normal direction of the target and thus the reflections cannot be

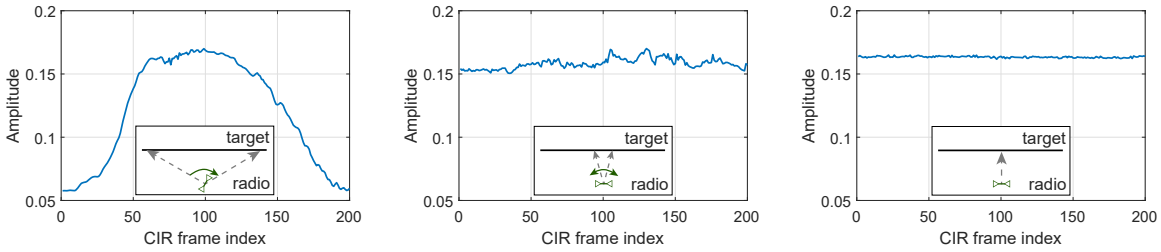

(a) Move from $-60°$ to $60°$ (b) Move between $(-10°, 10°)$ (c) Static at $0°$

Fig. 10. Measurements on specular reflection. The measurement setup is shown in respective figures: (a) The radio is rotated from an orientation of $-60°$ (relative to the normal direction of the target) all the way to $60°$. (b) The radio is swinging back and forth between $(-10°, 10°)$. (c) The radio is put static and perpendicular to the target (*i.e.*, $0°$ orientation).

captured. To see the impacts of small distortions, we swing the device back and forth between $-10°$ and $10°$ and illustrate the measurements in Fig. 10b. Comparing with Fig. 10c, we can see that the amplitude responses remain quite stable, with only minor variances added. Albeit a range of $10°$ might not be much, and a user still needs to operate carefully, this property improves the practicability against angle distortions, especially in mobile cases.

Operating Distance Ideally, the working range is equal to the device's operating range, which is specified as 10m and in reality works for up to about 4 meters [34]. To ensure reliable measurements in practice, however, we only restrict to a short range, *e.g.*, within a half meter. The reasons are two-fold: First, the signals become very noisy at distant ranges due to the high attenuation nature of 60GHz signals. Second, as shown in Fig. 9(b), although we can tolerate slight offsets of the device orientation in short ranges, these minute offsets will be amplified over large distances, especially in mobile scenarios. Consequently, we limit the operating range of `mSense` to a short but reasonable range. We note that such range constraints do not harm the practicability of `mSense` since material sensing, especially with a hand-held mobile device, is more likely performed within a short range than a long distance.

In practice, real-time feedback of the target distance could be provided for a user to hold and place the radio more appropriately. For example, a visual hint can be shown to guide the user to point the device to the empty space for calibration, and the system itself can detect if any target presents in a certain range for verification. In addition, the estimated target distance can be shown to instruct a user to move the device closer to (or farther away from) the target for better performance.

6 EXPERIMENTAL RESULTS

6.1 Experiment Methodology

Recall Fig. 3, our experiments are mainly conducted in two scenarios: 1) Static case: The device is put still (at different locations and distances) on top of a desk to sense a target; 2) Mobile case: A user holds the device in hand and/or moves it for a short distance while performing sensing. We first perform micro benchmark study by considering common materials, including metals (aluminum), plastics (acrylic), ceramics, water, and woods, and carry out daily object recognition in the next section. As shown in Fig. 11, the objects we use for micro benchmarks have different sizes and thicknesses. During data collection, the device is pointed to the surface of the target. In the case of water, we use a plastic container (about $6 \times 15 \times 18$ cm in size) and point the device down towards the top surface of the water. We mainly perform two data collection sessions over two different days and settings, denoted as dataset #1 and dataset #2 respectively for convenience. For each data session, we measure multiple sets of data for each material, each set containing 150 to 200 frames. The data are collected at

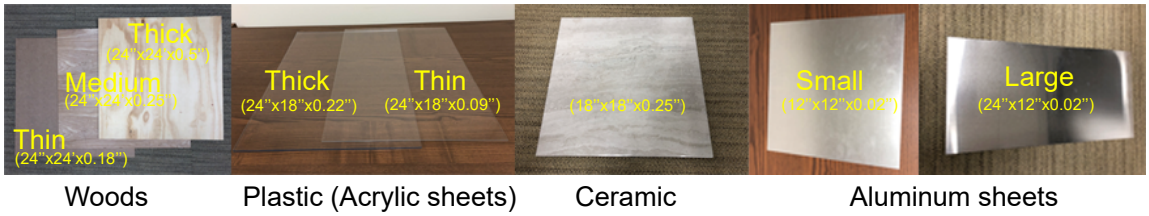

Fig. 11. Testing materials (water not shown)

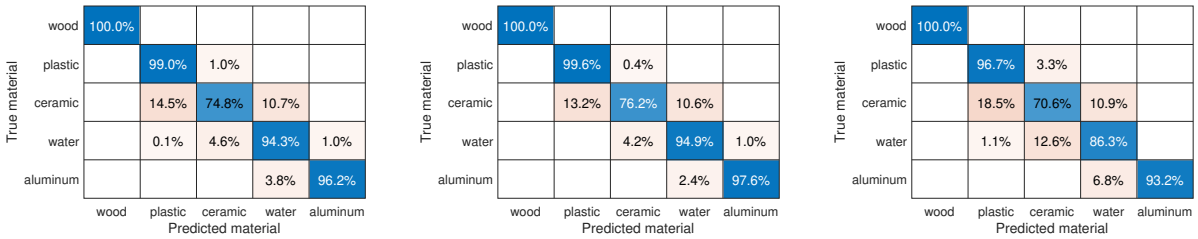

(a) Overall accuracy (b) Accuracy in static case (c) Accuracy in mobile case

Fig. 12. Overall accuracy.

multiple locations in a large office building. During each session, we only collect one set of the empty data for noise cancellation, while the device is allowed to move and change location. As a result, the data are collected with the device at different distances to the target and on slightly different orientations. We use all the available Tx and Rx elements for data collection, resulting in 32×32 CIR frames.

We train the MRF database using one dataset and test with the data from the other dataset, with no information leakage between the two datasets. For comprehension, we switch the training and testing datasets and integrate the results for each evaluation case. To facilitate the training, we employ a trick as follows for data augmentation, a common technique widely used in machine learning. Specifically, for each sample with 32 Tx antennas and 32 Rx antennas, we randomly drop out one antenna and generate a new sample on top, producing 64 extra samples for training. By doing this, we boost the training data size by 64 times, allowing much more realizations for a better histogram distribution.

6.2 Micro Benchmarks

Overall Performance We first present the overall recognition performance. We use two frames per sample for training, while average five frames as a testing sample (the impacts of the number of frames per sample will be evaluated subsequently). The results of both the mobile and static cases are fused together. As shown in Fig. 12a, the overall recognition accuracy is 92.87%, comparable to the existing works that need to penetrate the target with bilateral device setup and cannot be used for mobile material sensing [14, 30]. Specifically, `mSense` achieves a remarkable recognition accuracy exceeding 90% for all the tested materials except for ceramic, of which the estimated MRFs exhibit a larger variance and overlap with both plastic and water. And note that metals (*e.g.*, aluminum) are identified correctly with high accuracy, even in mobile cases, which would be particularly useful to detect suspicious targets for security [28]. We believe the accuracy promises valuable applications for ubiquitous contexts thanks to `mSense`'s simple setup of using single radio and reflection signals only.

Comparing static and mobile cases It is of particular interests to examine the performance of `mSense` in mobile environments. Thereby, as shown in Fig. 12b and Fig. 12c, we demonstrate the accuracy in mobile and

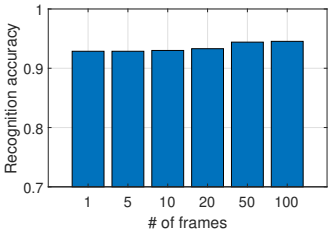

Fig. 13. Impacts of the number of frames

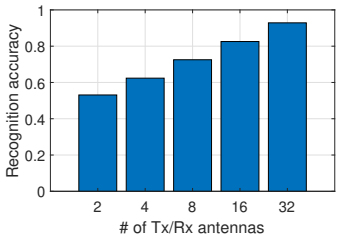

(a) Random selection

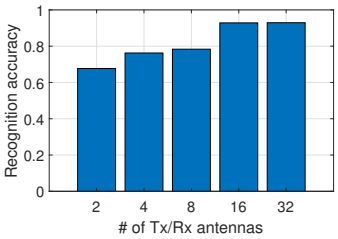

(b) Smaller subarray

Fig. 14. Impacts of antenna number

static scenarios separately. As seen, the performance in the static scenario is as expected slightly better than that in the mobile scenario, decreasing from 93.66% to 89.36%. The retained performance in mobile environments, with around 4% accuracy degradation, could still suffice many everyday applications.

The number of frames per sample We now analyze the impacts of the number of CIR frames used in one single query for testing. As shown in Fig. 13, we examine the recognition performance by increasing the number of frames from 1 all the way up to 100 per sample. The overall recognition accuracy correspondingly improves by a marginal gain from about 93% to 95%. Generally, the more frames are used, the better results can be obtained. Specifically, the accuracy achieves 94.41% when using 50 frames per sample, which is about 2.5 seconds on our current testbed with a sampling rate of about 20Hz. The sampling rate is mainly limited by the file and network I/O of the current implementation. Yet too many frames will cause larger delays and potentially involve larger distortions that might impair the accuracy. We default the number of frames per sample to five in `mSense` to trade off the accuracy with the measuring delay and computation. A shorter sensing time not only delivers better user experience but also allows more room for the networking counterpart in the joint radar communication systems.

Impact of antennas We use 32 Tx and Rx antennas to overcome the measurement noises and improve MRF estimation robustness. To quantify the effectiveness, we examine two cases: 1) selecting a random subset of antennas and 2) using a certain subset of a smaller size. As shown in Fig. 14a, the spatial diversity attributed by many antennas significantly improves the recognition accuracy. For example, the performance degrades to 82.57% when using 16 Tx and 16 Rx antennas. When using a fixed subset, as depicted in Fig. 14b, the performance decays more slowly, which keeps almost unimpaired with 16 antennas and drops below 80% with 8 antennas. The difference may be because, in the random selection case, different antenna sets may be used for the Tx and Rx, leading to asymmetric spatial diversity.

Impacts of sizes and thickness One critical issue of a general material sensing system is whether it can deal with various target sizes and thicknesses. We have involved targets with different sizes and thicknesses in our experiments. Specifically, we employ aluminum sheets with two sizes but the same thickness, plastic boards with different thicknesses, and wood panels with different thicknesses and surfaces but the similar sizes. To evaluate the performance, we exclude the testing type (*e.g.*, thick wood) in training and test it using the trained model. We repeat this procedure for different sizes and thicknesses and portray the recognition results in Fig. 15. As seen, `mSense` achieves consistently great accuracy, all beyond 95%, regardless of different sizes and thicknesses, indicating that it is independent from the target size and thickness and thus conforming to our analysis in Fig. 9.

Impacts of incident angles We have explained in Fig. 9 and Fig. 10 that `mSense` tolerates certain angle distortions. We now evaluate the impacts by examining the performance at different pointing angles from 0° to 20°. For each testing angle, we collect 200 samples and test against the model trained using the data measured at 0°. As shown in Fig. 16, the recognition accuracy degrades by about 15% when the incident angle deviates to 5° and 10° but is

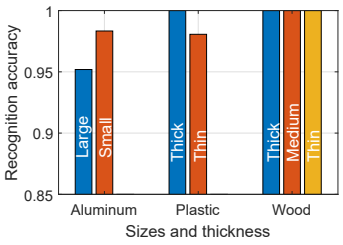

Fig. 15. Impacts of target sizes and thicknesses

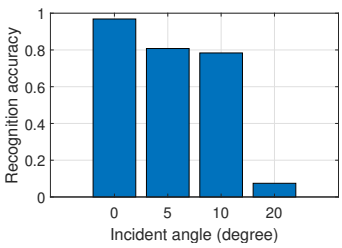

Fig. 16. Accuracy wrt. incident angle

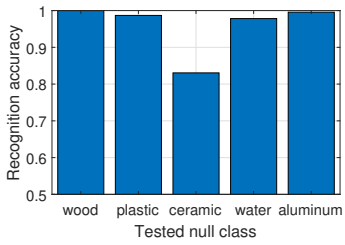

Fig. 17. Accuracy for unseen materials (null classes)

still acceptable. When operating at 20°, however, the received signals attenuate too much due to the unaligned incident and reflection angles, leading to reduced MRF values that may not be identified as the original material. As such, the operating range for the current system is recommended as about -10° to 10°. Compensating the gain in a specific direction based on the beam patterns might enlarge the operating angles, which keeps as future work. We also note that operation errors in angles may exist throughout our experiments, including this case itself.

Null class One common concern for material sensing is the null class issue, *i.e.*, how the system reacts to "unseen" objects. To evaluate mSense, we purposely exclude one of the five materials in training and test it against the re-trained model, which doesn't see any of this specific material (*i.e.*, a null class). Note that the training and testing samples are still from the different datasets. As illustrated in Fig. 17, mSense correctly detects the tested null classes with an average accuracy of 95.32%. The accuracy decreases to 83.05% when testing ceramic as the null class because, again, its MRF spans over those of water and plastic. We note that mSense's capability in handling unseen materials is limited by the resolution and robustness of the MRF. If a new material appears with very similar MRF to an existing one, mSense may wrongly declare it as a known type.

Runtime complexity We analyze the runtime complexity with our current MATLAB implementation of mSense on a Windows desktop with Intel Core i7 CPU@3.6GHz and 32GB RAM. The major system latency of our current implementation lies in the inefficient interpolation operation in MATLAB, which in average takes over 600 ms for each CIR frame. The other processing operations consume about 110 ms. We believe the latency will be largely reduced with a better implementation of the interpolation operation. And in practice, delays of seconds would be acceptable for applications like daily object recognition.

6.3 Material Recognition for Daily Objects

To test mSense's applicability to more real-life objects, we carry out a case study for a set of daily objects made of different complex materials and various sizes, surfaces, shapes, etc. We involve 21 different everyday objects including tables and chairs, building materials, kitchen utensils, toys, etc. The materials include different woods, plastics, foams, glasses, metals, and complex mixed ones. As shown in Fig. 18, we present the material compositions as detailed as we can source (some are still missing since we do not have the exact information). All the objects are used items in real life and are in different conditions. For each material, we collect 1600 frames over different times across three days, which result in 320 samples. The objects are sampled over different locations within a typical 2-bedroom apartment. We use 25% of the data for training and the rest for testing and shuffle for 10 folds to obtain the results.

As seen in Fig. 18, most objects of similar materials are correctly recognized as the same basic types. For example, metal objects (the red box area in Fig. 18) are nearly 100% identified. Wooden items (the green box area) and plastic items (the blue box area) are also reliably classified into the correct groups. However, the recognition accuracy for individual objects does decrease, as expected, when more targets and more similar materials are

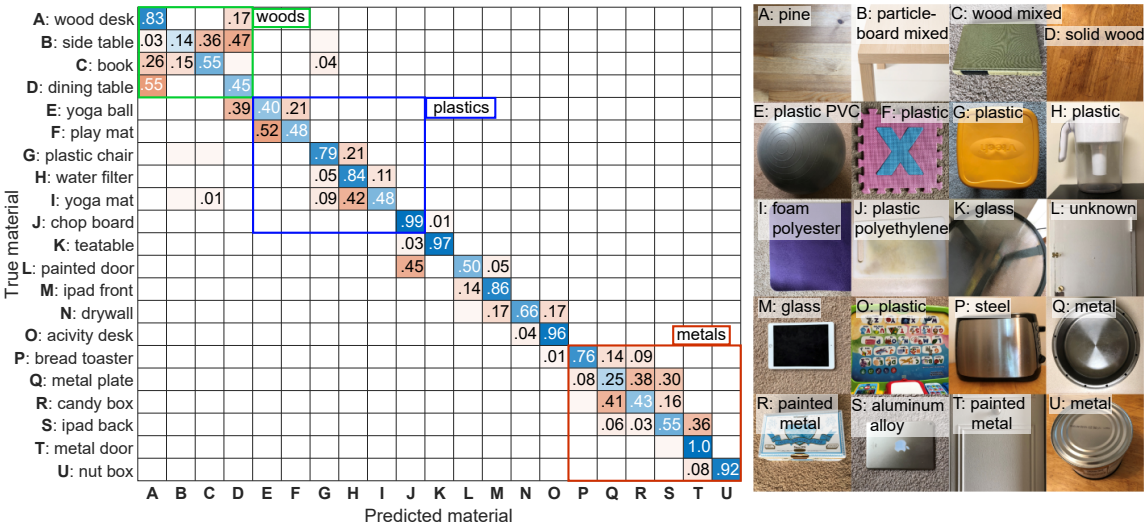

Fig. 18. Daily object recognition

involved. The ability to distinguish objects of similar materials depends on how different the specific materials' reflectivity is. For example, object K and M are both made of glass but are clearly classified. Differently, metal objects Q and R are similar to each other, while items T and U, also metals, are again distinguishable. Confusion between such objects is by their similar reflection, which results in too close MRF values. Similar confusion will persist due to overlapped material features even using the penetration signals to estimate the precise permittivity [12]. The considerable noises on our testbed device, even after our processing, also increase the confusion.

More importantly, Fig. 18 also demonstrates that mSense tolerates targets of different surface textures, shapes, sizes, hardness, etc. The objects tested have coarse surfaces (*e.g.*, chopping board, painted walls) or fine ones (*e.g.*, iPad), and could be soft (*e.g.*, play/yoga mat) or hard (*e.g.*, metal plate). Objects with irregular shapes (*e.g.*, the yoga ball, bread toaster, and water filter all have curved surface) are also considered. Furthermore, they could be composed of single materials (*e.g.*, metal plate) or mixed materials (*e.g.*, painted drywalls and metal boxes). But there appear to be no noticeable impacts of these factors on the recognition. However, we note that mSense cannot handle very flexible objects. We have tested a relatively soft mattress (covered by a thin cotton sheet) but do not get consistent reflection measurements because the shape likely has changed over different samples. Sensing objects of flexible surfaces is a future direction to explore for more materials such as various fabrics.

7 DISCUSSIONS AND LIMITATIONS

By designing mSense, our main goal is to demonstrate the feasibility of daily material identification using reflection signals only. As an early step, there is room for improvements of the current system. First, limited by the potentially close reflection of different objects and the measurement noises on our testbed, mSense cannot distinguish very similar materials, but only classifies them as the same material type. The distinction between similar objects would be useful, *e.g.*, for verifying the solid wood type or the fabric type of clothing in a store, which we keep as future work. Second, mSense cannot sense an occluded target. While 60GHz signals barely penetrate many objects, we plan to explore the feasibility of two special Non-LOS cases, *i.e.*, through-the-paper-box and through-the-liquid-bottle sensing, without opening the containers or instrumenting the them. Third, we mainly focus on targets with a relatively (but not necessarily perfectly) flat surface. Handling various surfaces

Table 1. A comparison of related methods.

	Radio	# of device	Signals	Setup	Materials	Accuracy
TagScan [30]	RFID	3	Penetration	Two-sided	10 liquids, 6 solids	>94%
TagTag [35]	RFID	3	Reflection	Instrumented	16 liquids, 7 solids	94%
WiMi [14]	WiFi	2	Penetration	Two-sided	10 liquids	96%
IntuWition [39]	WiFi	4	Reflection	Portable	5 types	95%
LiquID [12]	UWB	2	Penetration	Two-sided	33 liquids	N/A
RadarCat [37]	Soli	1	Touch-based	Portable	26 objects	99.97%
mSense	mmWave	1	Reflection	Portable	5 types, 21 objects	93%

and shapes, *e.g.*, soft and flexible clothes, remains an open issue. Finally, since we use the reflection signals, we are technically sensing the surface material yet do not identify the internal one, be it different from the surface.

8 RELATED WORKS

Material Identification Conventional and commercial systems for material imaging and identification employ techniques like optical spectroscopy, large radar, X-Ray, CT/MRI, etc. Despite of high-resolution results, these systems need specialized instrument that is bulky and costly, limiting them to only lab environments and critical security usage. Enabling material identification in a more ubiquitous setting emerges as an increasingly hot topic in the last few years [12, 30, 37, 38].

Many works resort to RF signals, as summarized in Table 1. Efforts are particularly devoted to liquid identification. LiquID [12] achieves high accuracy for liquid testing using UWB radar under a dedicated setup with a special container. TagScan [30] classifies liquids by using phase and RSS changes of RFID signals that penetrate through the target. A later work TagTag [35] leverages the impedance change of RFID tags attached to the target and can sense multiple targets simultaneously. RFIQ [16] exploits electromagnetic interactions between RFID tags placed on the container and the materials inside to sense food quality. TwinLeak [15] uses RFID to detect liquid leakage but does not identify the liquid types. WiFi signals are also exploited for material sensing. WiMi [14] implements a similar idea of TagScan [30] on commodity WiFi devices to identify liquids. A suspicious object detection system is designed in [28] by detecting liquids and metals from other objects. Strobe [13] senses soil moisture using a WiFi receiver buried in the soil. IntuWition [39] leverages 3 mutually perpendicular receive antennas (built from three commodity WiFi cards) to recognize materials, which is so far the only work using reflection signals on WiFi. Millimeter-wave radios, including dedicated radar [10, 37] and networking devices [44, 45], have been used for object imaging and recognition. RadarCat [37] employs the Google Soli [18] to touch the targets, but identifies different objects of the same material type as different materials. [10] trains a neural network with raw signals from a UWB Radar. RSA [45] focuses on imaging with 60GHz radios, yet requires the Tx and Rx to be well separated and moving independently. Ulysses [44] improves RSA by using a single device, but still needs to move the radio precisely and does not suit hand-held mobile scenarios. Unlike existing works, mSense reuses a single commodity mmWave networking device and exploits the reflection signals to extract explainable and distinguishable features for material sensing.

Wireless Sensing In addition to material identification, wireless sensing has been widely studied for various applications [9, 11, 20, 21, 32, 33]. Specifically, researchers have been leveraging WiFi signals for human tracking [25], motion detection [40], breathing and sleep monitoring [41], gesture recognition [24, 43], fall detection [29], activity recognition [31], RF imaging [8], etc. Recently, mmWave signals are also exploited for passive localization [34], vital sign monitoring [36], gesture recognition [18], etc. The main body of existing work focuses on human-centric sensing with special interests in location and motion contexts. Conversely, this work studies material identification of everyday objects.

Radar-Communication Coexistence The synergistic design of communication and radar systems [19, 42] emerges to utilize common spectral and hardware resources to enable dual functions in one single system, permitting a new paradigm of efficiently utilizing the limited RF spectrum [17]. Particularly, the millimeter-wave band arising as a preferred technology for short-distance high-throughput networking technique also promises radar sensing applications [22]. We categorize our testbed as an early attempt in this theme. Yet we mainly focus on its radar perspective and specifically demonstrates the feasibility of material sensing on top in this work. We believe our practice would greatly benefit the community of both wireless sensing and networking.

9 CONCLUSION

This paper presents mSense, a first-of-its-kind system that senses the material type of daily objects via RF signals reflected off the target by reusing a commercial 60GHz networking chipset as a mmWave radar-like radio. It introduces a novel material reflection feature that characterizes the material's intrinsic reflectivity and thus associates with specific material type. Experimental evaluation on common materials demonstrates high accuracy in both static and mobile scenarios. A case study further validates the applicability to real-life recognition of daily objects. mSense not only promises mobile and ubiquitous material identification for everyday objects but also inspires how future research can reuse mmWave networking devices for sensing.

ACKNOWLEDGMENTS

The authors thank Qualcomm for providing the 60GHz testbed on which our experiments were carried out, the anonymous reviewers and editors for their valuable comments, and the Origin Wireless team for their support.

REFERENCES

[1] 2018. 60-GHz Wi-Fi Gets a Refresh: Qualcomm Rolls Out Chips for 802.11ay. https://www.eetimes.com/document.asp?doc_id=1333870.
[2] 2018. Asus Foreshadows 5G Handsets Featuring 802.11ad WiFi. https://www.eetimes.com/author.asp?section_id=36&doc_id=1333373.
[3] 2018. Qualcomm 60GHz WiGig/WiFi 802.11ad Chipset World's First Smartphone Edition Complete Teardown Report. https://www.researchandmarkets.com/research/3klmm4.
[4] 2019. Google's Project Soli: The Tech Behind Pixel 4's Motion Sense Radar. https://www.theverge.com/2019/10/15/20908083/google-pixel-4-project-soli-radar-motion-sense-explainer.
[5] 2019. Qualcomm 802.11ad 60GHz WiFi. https://www.qualcomm.com/solutions/networking/features/80211ad.
[6] 2019. Talon AD7200 Multi-Band Wi-Fi Router. https://www.tp-link.com/us/home-networking/wifi-router/ad7200/.
[7] 2019. The Biggest iPhone News Is a Tiny New Chip Inside It. https://www.wired.com/story/apple-u1-chip/.
[8] Fadel Adib, Chen-Yu Hsu, Hongzi Mao, Dina Katabi, and Frédo Durand. 2015. Capturing the human figure through a wall. *ACM Transactions on Graphics* 34, 6 (2015), 219.
[9] Fadel Adib, Zachary Kabelac, and Dina Katabi. 2015. Multi-person localization via RF body reflections. In *Proceedings of USENIX NSDI*.
[10] Gianluca Agresti and Simone Milani. 2019. Material Identification Using RF Sensors and Convolutional Neural Networks. In *Proceedings of IEEE ICASSP*. IEEE, 3662–3666.
[11] Maurizio Bocca, Ossi Kaltiokallio, Neal Patwari, and Suresh Venkatasubramanian. 2013. Multiple target tracking with RF sensor networks. *IEEE Transactions on Mobile Computing* 13, 8 (2013), 1787–1800.
[12] Ashutosh Dhekne, Mahanth Gowda, Yixuan Zhao, Haitham Hassanieh, and Romit Roy Choudhury. 2018. LiquID: A Wireless Liquid IDentifier. In *Proceedings of ACM MobiSys*. ACM, 442–454.
[13] Jian Ding and Ranveer Chandra. 2019. Towards Low Cost Soil Sensing Using Wi-Fi. In *Proceedings of ACM MobiCom*. ACM, 1–16.
[14] Chao Feng, Jie Xiong, Liqiong Chang, Ju Wang, Xiaojiang Chen, Dingyi Fang, and Zhanyong Tang. 2019. WiMi: Target Material Identification with Commodity Wi-Fi Devices. In *Proceedings of IEEE ICDCS*. IEEE, 700–710.
[15] Junchen Guo, Ting Wang, Yuan He, Meng Jin, Chengkun Jiang, and Yunhao Liu. 2019. Twinleak: Rfid-based liquid leakage detection in industrial environments. In *Proceedings of IEEE INFOCOM*. IEEE, 883–891.
[16] Unsoo Ha, Junshan Leng, Alaa Khaddaj, and Fadel Adib. 2020. Food and Liquid Sensing in Practical Environments using RFIDs. In *Proceedings of USENIX NSDI*.
[17] Aboulnasr Hassanien, Moeness G Amin, Elias Aboutanios, and Braham Himed. 2019. Dual-Function Radar Communication Systems: A solution to the spectrum congestion problem. *IEEE Signal Processing Magazine* 36, 5 (2019), 115–126.

[18] Jaime Lien, Nicholas Gillian, M Emre Karagozler, Patrick Amihood, Carsten Schwesig, Erik Olson, Hakim Raja, and Ivan Poupyrev. 2016. Soli: Ubiquitous gesture sensing with millimeter wave radar. *ACM Transactions on Graphics* 35, 4 (2016), 142.

[19] Fan Liu, Longfei Zhou, Christos Masouros, Ang Li, Wu Luo, and Athina Petropulu. 2018. Toward dual-functional radar-communication systems: Optimal waveform design. *IEEE Transactions on Signal Processing* 66, 16 (2018), 4264–4279.

[20] K. J. Ray Liu and Beibei Wang. 2019. *Wireless AI: Wireless Sensing, Positioning, IoT, and Communications*. Cambridge University Press.

[21] Adrian Loch, Hany Assasa, Joan Palacios, Joerg Widmer, Hans Suys, and Björn Debaillie. 2017. Zero overhead device tracking in 60 GHz wireless networks using multi-lobe beam patterns. In *Proceedings of ACM CoNext*. ACM, 224–237.

[22] Kumar Vijay Mishra, MR Bhavani Shankar, Visa Koivunen, Bjorn Ottersten, and Sergiy A Vorobyov. 2019. Toward Millimeter-Wave Joint Radar Communications: A signal processing perspective. *IEEE Signal Processing Magazine* 36, 5 (2019), 100–114.

[23] Ioannis Pefkianakis and Kyu-Han Kim. 2018. Accurate 3D localization for 60 GHz networks. In *Proceedings of ACM SenSys*. ACM, 120–131.

[24] Qifan Pu, Sidhant Gupta, Shyamnath Gollakota, and Shwetak Patel. 2013. Whole-home gesture recognition using wireless signals. In *Proceedings of ACM MobiCom*. ACM, 27–38.

[25] Kun Qian, Chenshu Wu, Yi Zhang, Guidong Zhang, Zheng Yang, and Yunhao Liu. 2018. Widar2. 0: Passive human tracking with a single wi-fi link. In *Proceedings of ACM MobiSys*. ACM.

[26] Arthur Robert Von Hippel. 1954. *Dielectrics and waves*. Wiley. 3 – 28 pages.

[27] Beibei Wang, Qinyi Xu, Chen Chen, Feng Zhang, and K J Ray Liu. 2018. The promise of radio analytics: a future paradigm of wireless positioning, tracking, and sensing. *IEEE Signal Processing Magazine* 35, 3 (2018), 59–80.

[28] Chen Wang, Jian Liu, Yingying Chen, Hongbo Liu, and Yan Wang. 2018. Towards in-baggage suspicious object detection using commodity WiFi. In *Proceedings of IEEE CNS*. IEEE, 1–9.

[29] Hao Wang, Daqing Zhang, Yasha Wang, Junyi Ma, Yuxiang Wang, and Shengjie Li. 2016. RT-Fall: A real-time and contactless fall detection system with commodity WiFi devices. *IEEE Transactions on Mobile Computing* 16, 2 (2016), 511–526.

[30] Ju Wang, Jie Xiong, Xiaojiang Chen, Hongbo Jiang, Rajesh Krishna Balan, and Dingyi Fang. 2017. TagScan: Simultaneous target imaging and material identification with commodity RFID devices. In *Proceedings of ACM MobiCom*. ACM, 288–300.

[31] Wei Wang, Alex X Liu, Muhammad Shahzad, Kang Ling, and Sanglu Lu. 2015. Understanding and modeling of wifi signal based human activity recognition. In *Proceedings of ACM MobiCom*. ACM, 65–76.

[32] Chenshu Wu, Zheng Yang, Zimu Zhou, Xuefeng Liu, Yunhao Liu, and Jiannong Cao. 2015. Non-invasive detection of moving and stationary human with wifi. *IEEE Journal on Selected Areas in Communications* 33, 11 (2015), 2329–2342.

[33] Chenshu Wu, Feng Zhang, Yusen Fan, and K. J. Ray Liu. 2019. RF-based Inertial Measurement. In *Proceedings of ACM SIGCOMM*. ACM, 117–129.

[34] Chenshu Wu, Feng Zhang, Beibei Wang, and K. J. Ray Liu. 2020. mmTrack: Passive Multi-Person Localization Using Commodity Millimeter Wave Radio. In *Proceedings of IEEE INFOCOM*.

[35] Binbin Xie, Jie Xiong, Xiaojiang Chen, Eugene Chai, Liyao Li, Zhanyong Tang, and Dingyi Fang. 2019. Tagtag: material sensing with commodity RFID. In *Proceedings of ACM SenSys*. ACM, 338–350.

[36] Zhicheng Yang, Parth H Pathak, Yunze Zeng, Xixi Liran, and Prasant Mohapatra. 2016. Monitoring vital signs using millimeter wave. In *Proceedings of ACM MobiHoc*. ACM.

[37] Hui-Shyong Yeo, Gergely Flamich, Patrick Schrempf, David Harris-Birtill, and Aaron Quigley. 2016. Radarcat: Radar categorization for input & interaction. In *Proceedings of ACM UIST*. ACM, 833–841.

[38] Shichao Yue and Dina Katabi. 2019. Liquid Testing with Your Smartphone. In *Proceedings of ACM MobiSys*. ACM, 275–286.

[39] Diana Zhang, Jingxian Wang, Junsu Jang, Junbo Zhang, and Swarun Kumar. 2019. On the Feasibility of Wi-Fi Based Material Sensing. In *Proceedings of ACM MobiCom*. ACM, 41.

[40] Feng Zhang, Chenshu Wu, Beibei Wang, Hung-Quoc Lai, Yi Han, and K J Ray Liu. 2019. WiDetect: Robust Motion Detection with a Statistical Electromagnetic Model. *Proceedings of the ACM on Interactive, Mobile, Wearable and Ubiquitous Technologies* 3, 3 (2019), 1–24.

[41] Feng Zhang, Chenshu Wu, Beibei Wang, Min Wu, Daniel Bugos, Hangfang Zhang, and K J Ray Liu. 2019. Smars: sleep monitoring via ambient radio signals. *IEEE Transactions on Mobile Computing* (2019).

[42] Le Zheng, Marco Lops, Yonina C Eldar, and Xiaodong Wang. 2019. Radar and Communication Coexistence: An Overview: A Review of Recent Methods. *IEEE Signal Processing Magazine* 36, 5 (2019), 85–99.

[43] Yue Zheng, Yi Zhang, Kun Qian, Guidong Zhang, Yunhao Liu, Chenshu Wu, and Zheng Yang. 2019. Zero-effort cross-domain gesture recognition with Wi-Fi. In *Proceedings of ACM MobiSys*. ACM, 313–325.

[44] Yanzi Zhu, Yuanshun Yao, Ben Y Zhao, and Haitao Zheng. 2017. Object recognition and navigation using a single networking device. In *Proceedings of ACM MobiSys*. ACM, 265–277.

[45] Yanzi Zhu, Yibo Zhu, Ben Y Zhao, and Haitao Zheng. 2015. Reusing 60ghz radios for mobile radar imaging. In *Proceedings of ACM MobiCom*. ACM, 103–116.